Nanostructured Electrodes for High-Performing Solid Oxide Fuel Cells

8

Hanping Ding

Contents

Abstract

Solid oxide fuel cell (SOFC) is an all-solid-state ceramic electrochemical device for converting chemical energy (fuels) to electricity with high energy efficiency and ultralow harmful emissions. These classes of FCs have received significant attention by researchers as a potential replacement for petroleum-based energy devices. In order to broaden the material selection and increase material system durability, the development of intermediate- or low-temperature SOFC is critical to making their commercialization viable. Therefore, the SOFC performance at lowered operating

Author Contributions

Dr. Ding would like to thank Prof. Neal P. Sullivan, the Director Colorado Fuel Cell Center, for providing numerous supports during author's academic stay in Colorado School of Mines.

H. Ding (✉)
Department of Mechanical Engineering, Colorado Fuel Cell Center, Colorado School of Mines, Golden, CO, USA

Energy & Environmental Science and Technology, Idaho National Laboratory, Idaho Falls, USA
e-mail: hanpingding@gmail.com; Hanping.ding@inl.gov

F. Li et al. (eds.), *Nanostructured Materials for Next-Generation Energy Storage and Conversion*, https://doi.org/10.1007/978-3-662-56364-9_8

temperatures must be improved by the innovation of materials and microstructures. The nanostructure engineering of electrodes has demonstrated their improved catalytic performance due to minimization of the electrode polarization resistances for oxygen reduction reaction and fuel oxidation reaction at the nanoscale compared to the traditional electrode design. The synthesis technique strategy was based on wet chemistry catalyst infiltration into electrode structure and has been demonstrated improvements in power density and electrode stability. In this chapter, the technical process of ion infiltration method is discussed; and the different routes in fabricating nanostructured electrodes to achieve high-performing SOFC in hydrogen and hydrocarbon fuels are reviewed. The electrode parameters that lead to improvement of SOFC performance are also summarized. By fabricating electrodes at the nanoscale, a significant increase in specific area was obtained that can provide greater active catalysis sites for electrode reactions, as well as a decrease in the activation polarization resistance which collectively led to improved SOFC performance.

8.1 Introduction

The solid oxide fuel cell (SOFC) is an attractive technology for chemical-to-electrical energy conversion due to its advantages such as high efficiency, low operation cost, and fuel flexibility [1–4]. As a ceramic device, the FC operates at a high temperature which facilitates its high efficiency when combined with a gas turbine. The absence of expensive catalyst material and resistance against fuels containing carbon monoxide contributes to its lower manufacturing cost [5–7]. Investigators have aimed to increase SOFC power efficiencies from a variety of fuel feedstocks through research and development of functional materials used in SOFCs. Researchers have focused on new cell design; fabrication of composite electrode or new electrode structures, mathematical analysis of gas flow patterns, and thermodynamic modeling of catalysis at the electrode surface are examples of areas of research which will lead to improvements in FC electrochemical performance. The higher operating temperature also requires the FC design to incorporate materials that result in increased physical and chemical compatibility with other cell components, the capability of system incorporation into the stack, which in turn enables the FC to be operated at a lower temperature increasing long-term FC stability [8–10]. The commercialization trend of an SOFC system for distributed power sources has become more widespread, due to improvements in optimized operating conditions, resulting in better longevity and lower manufacturing costs. At present, while this technology exhibits great promise to be applied in society, there remain three major engineering and scientific hurdles. Firstly, the relative high operating temperature requires the SOFC materials and other key components in the stacks such as sealing and interconnecting materials to be compatible resulting in increased reliability of the stack system [11, 12]; secondly, the use of petroleum-based fuels faces technical problems such as coking and sulfur poisoning when nickel-based anode catalysts are used, although researchers have proposed some strategies to avoid the degradation of FCs when using fuels containing carbon and sulfur [13–15]; thirdly, the higher operating temperature leads to a

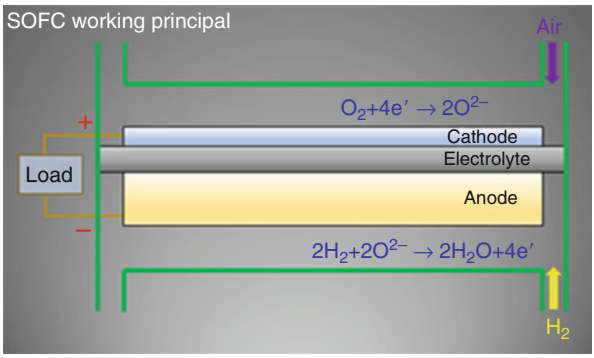

Fig. 8.1 The working principle of a solid oxide fuel cell (SOFC)

degradation in performance over time affecting their longevity, and contributing to increased manufacturing and maintenance costs, and ultimately FC efficiency [16, 17]. Therefore, researchers have focused efforts on developing materials and structures and operating conditions that have been made to optimize the performance of single-cell level and stack compatibility [18, 19]. Since the high operating temperature restricts potential SOFC material selection and reliability, various technical routes have been explored to increase FC robustness and performance. The introduction of more active catalysts, or catalyst with an increased specific surface, and more conductive materials is shown to contribute to improved FC electrochemical performance at lower temperatures.

A typical oxide-ion conducting-based SOFC is composed of two electrodes and one electrolyte (Fig. 8.1). The oxygen ions are formed by oxygen molecules associating with two electrons at the cathode compartment that is transported through the dense electrolyte to reach the anode compartment. The oxygen ions can react with hydrogen fuel to form the water. During this process, the electrons released from hydrogen pass through the external circuit to form the electricity. The SOFC performance is directly determined by the internal resistance which is related with the overpotential polarization of each component contributed by imperfections in materials, microstructure, and design of the fuel cell [20]. There are three main polarization resistances contributed by different physical or electrochemical phenomenon: ohmic resistance, concentration polarization, and activation polarization.

Firstly, the ohmic resistance is determined by the conductivities of these three components. The resistance is mainly determined by the electrolyte material since the electronic conductivities of the cathode (usually conductive oxide) and anode (nickel metal in cermet composite) are several magnitudes higher than that of electrolyte which is ionic and conductive in nature.

Therefore, the ohmic resistance of electrolyte dominates the total resistance; consequently, the conductivity and thickness of the electrolyte become two important parameters to control the resistance. The electrolyte resistance can be minimized through the incorporation of high conductive electrolyte materials and techniques for fabricating thin membranes. Secondly, the concentration polarization resistance results from limitations on the mass transport within the electrode structure [21, 22].

The reactants may be consumed by the electrochemical reaction faster than they can diffuse into the reaction boundaries, which causes the reactant concentration to be lower than required for optimal performance. The concentration polarization occurs in both the anode and cathode compartments. This polarization is in part due to electrode design that is very thin and highly porous. The reaction products of steam can dilute the fuel stream which must transport through the whole anode substrate to the three-phase boundary. The relevant optimization strategies of anode microstructure such as increasing porosity and grade electrode can decrease this polarization resistance significantly with the compromise of other properties. Lastly, the activation polarization is the result of catalytic activity toward oxygen reduction reaction (ORR) and fuel oxidation reaction, which is closely related to the catalytic activity of the employed materials and microstructure [23].

In a typical anode-supported SOFC with electrolyte thin membrane operated in hydrogen, the cell performance is affected by the ohmic resistance of electrolyte film and activation resistance from cathode material. The electrolyte resistance can be significantly reduced by using very thin film, and concentration polarization can be decreased by optimizing the microstructure for improved gas diffusion; the cathode activation polarization is the dominant factor in the total cell resistance. Therefore, the development of highly active materials and optimal electrode morphology is critical to improving the FC performance. Therefore the relationship of good material candidates to improved electrochemical catalysis requires improvements in oxygen diffusion efficiency and increased surface exchange kinetics, which are empirically or experimentally associated with mixed electrical conductivity. Researchers have significant efforts in developing newer cathode materials with high catalytic activity for oxygen reduction reaction (ORR) [24–26]. Many types of materials such as perovskite, spinel, and layered perovskite have been demonstrated as promising cathodes for high-performing SOFC [27–30]. In direct hydrocarbon-fueled SOFC with ceramic oxide anode, performance is constrained by the degree of electrode polarization resistance arising from both the cathode in the oxidizing condition and anode in the reducing atmosphere. Therefore, the propensity of ceramic oxide anode as a catalyst under complex gaseous conditions requires a greater understanding of catalyst kinetics, materials engineering, and electrode design for enhanced catalysis. There are several material candidates that are being developed for stable operation SOFC in hydrogen, methane, and other hydrocarbon fuels in the form of nanostructured catalysts [31–33].

Nano-engineering of the cathode electrode to form nano-network has been shown to significantly increase the ORR through the availability of more active sites at the electrode surface that in turn lead to increased SOFC performance. The conventional cathode layer is prepared by sintering the ceramic particles to form a porous electrode microstructure for gaseous diffusion and reaction. The length of three-phase boundaries for ORR reaction is closely related to electrochemical performance. To maximize the three-phase boundaries (TPBs) for high-performing SOFC, a new cathode structure with the higher specific surface area can be achieved by various technique routes, which enable nanostructured catalyst to be fabricated. The introduction of the nano-sized catalyst into the cathode backbone has been regarded as an effective way

to increase the surface area and ultimately FC performance [34–37]. There are many methods to embed the catalyst metal into the nano-network for increased SOFC performance [38–40]. The ion filtration or impregnation method via metal salt solution implanting into electrode structure attracts increasing attention and becomes the most effective way to develop a catalytic nano-network for extremely extended reaction sites. The ion filtration method can not only increase the specific surface area but also effectively avoid thermal or chemical compatibility problems between cathode and electrolyte. The technique of ion infiltration and development status, as well as perspective, is introduced and reviewed [41–44]. The significant increase of active sites for ORR or fuel oxidation in SOFC nanostructured electrodes can enhance catalytic activity with decreased electrode polarization resistance. The development status of nanostructured electrodes for high-performing SOFC operated in various fuels is discussed in this chapter.

8.2 Nanostructured Cathode for High-Performing Solid Oxide Fuel Cell (SOFC)

8.2.1 Embedding of Catalyst Nano-network into Cathode by Infiltration Method

Conventional cathode sintering requires high temperature to facilitate good mechanical bonding and necking between cathode and electrolyte, which cause rough microstructure with large particle size. The basic process of ion infiltration method is to deposit two-dimensional or three-dimensional catalysts into cathode layer by firing aqueous metal ion solution with fast ramping rate to control nuclei rate. The nano-network is vulnerable to the high temperature; therefore, it demands a new route to obtaining nano-sized catalyst in the cathode: (a) the conducting electrolyte or electrode backbone/framework is sintered onto electrolyte at normal sintering temperature; and (b) nano-sized catalysts are impregnated into the rigid electrode structure at low temperatures afterward. The nanostructured cathode is formed after this two-step preparation (Fig. 8.2). For yttria-stabilized zirconia (YSZ)-based cell,

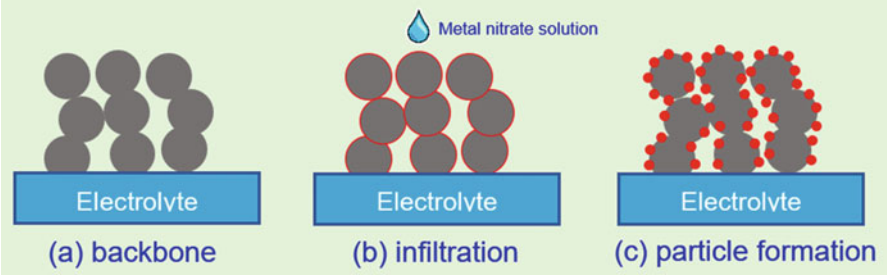

Fig. 8.2 The typical process of infiltration method: (**a**) YSZ backbone; (**b**) dropping solution onto particle surface; (**c**) formation of catalyst particles

for example, (a) the pure and porous YSZ structure with thickness about 10–30 μm was firstly deposited onto YSZ electrolyte after sintering at 1100–1200 °C; (b) the prepared solution with stoichiometric amount of metal salts for a specific chemical composition (e.g., lanthanum strontium manganite, LSM) is dipped into the YSZ backbone and then fired at relatively low temperature of 700 °C to form the LSM nanoparticles; and (c) the loading of LSM cathode particles is controlled by the infiltration cycling times.

There are several technical advantages for this infiltration method: (a) the generated nano-network can be well maintained at the relatively low formation temperature, while good mechanical strength between electrode and electrolyte is reached by the backbone layer; (b) the form of nano-network can be differentiated by various preparation conditions, such as heating/cooling rate and concentration of the metal nitrate solution, and (c) diverse materials with compositional complexity can be in situ synthesis and sintered in the electrode. For the different conducting interface required for ORR, two kinds of electrode structures are fabricated. If the cathode is composed of a pure electronic conductive material, a porous electrolyte scaffold/skeleton is fabricated on the dense electrolyte first to form oxide-ion conducting path, and then the cathode catalyst of nano-sized particles or wires is deposited onto the surface to extend the reaction TPB to the whole surface of electrolyte/electrode interface.

If the cathode is a mixed ionic-electronic conductor, there are two possible ways to fabricate the cathode. First, the scaffold can be the electrolyte for conducting only oxygen ions or mixed ionic-electronic conductors (MIEC) cathode for conducting both ions and electrons. The second step is to infiltrate the cathode catalyst onto the scaffold so that both backbone and surface catalyst can conduct electrons and ions simultaneously while ORR takes place on the nanoparticles.

8.2.2 Performance Improvements by Infiltrated Cathode

Many catalytically active oxides have been developed as the cathode materials for SOFC, in which perovskite structure is commonly used due to the capability of accepting oxygen vacancies readily and electronic conductivity by multivalent transition metals. Examples of perovskite-based cathode materials include lanthanum strontium manganite (LSM, $La_{0.8}Sr_{0.2}MnO_3$) [45], lanthanum strontium cobaltite (LSC, $La_{0.6}Sr_{0.4}CoO_3$) [46], samaria strontium cobaltite (SSC, $Sm_{0.5}Sr_{0.5}CoO_3$) [47], and barium strontium cobalt ferrite (BSCF, $Ba_{0.5}Sr_{0.5}Co_{0.8}Fe_{0.2}O_3$) [48]. The electrode backbone can be electrolyte material with ionic conduction or mixed ionic and electronic conductor.

In the conventional LSM-based cathode, the fluorite-structured yttrium-stabilized zirconia YSZ is introduced to the LSM nanoparticles by impregnation. The fabrication of such composite cathode can not only increase the reaction sites for oxygen reduction, but the materials also enhance the mechanical adhesion between electrode and electrolyte since the YSZ backbone is sintered at high temperature to easily form the good ceramic necking. Furthermore, the low-phase formation temperature can

also avoid the potential chemical reaction of LSM and YSZ in the case of direct sintering of composite electrode. He and Gorte et al. prepared LSM with perovskite phase by infiltrating mixed nitrate solution into a porous YSZ matrix, followed by a sintering process at various temperatures [49]. With uniform fine LSM particles, the electrical conductivity at 700 °C in the air with a porosity of 28% reached 3.16 S/cm. The cathode polarization resistance can be decreased to 0.5 $\Omega \cdot cm^2$ [50]. The anode-supported single cell with such fabricated cathode exhibited about 360 $mW \cdot cm^{-2}$ at 700 °C in humidified H_2. Armstrong and Virkar et al. also prepared infiltrated LSM electrode using nitrate-salt solution and achieved power density as high as 1.2 $W \cdot cm^{-2}$ for a cell operating in hydrogen at 800 °C [51]. Jiang et al. found that a proper chelating agent should be added to the nitrate solution to avoid segregation of individual metal ions during firing process to form pure LSM phase structure [52]. Because the infiltration process is an in situ wet chemistry method, the mobility of different metal ions can be reduced by encircling stable metal-chelate complexes steadily into the backbone by growing polymer network. For example, by using Triton X-100 as a chelating agent and one-step infiltration process, the LSM particles with a size of 30–100 nm were deposited on the outer wall of the pre-sintered porous YSZ, which provided a high density of active sites for oxygen reduction reaction [53]. A power density of 0.3 $W \cdot cm^{-2}$ at a low temperature of 650 °C was obtained. Furthermore, the infiltrated LSM nanoparticles were demonstrated to be electrochemically stable for 500 h at 650 °C when the cell was discharged at 150 $mA \cdot cm^{-2}$ [54].

As a mixed ionic and electronic conductor (MIEC), lanthanum strontium cobaltite (LSC) is a highly conductive perovskite material that has been used as a cathode material. To increase catalysis, the specific area of the catalyst area was increased by the design of a tubular structure. The LSC cathode was synthesized by using a pore-wetting technique [55]. The LSC nanotube yielded low electrode polarization resistance of 0.21 $\Omega \cdot cm^2$ at 700 °C measured from the prepared symmetric cell. However, the LSC cathode was not very stable under cathodic conditions. Huang et al. proved that the high ORR activity could be retained by coating the surface with a conformal layer of nanoscale zirconia (ZrO_2) film by atomic layer deposition (ALD) method [56]. The nanostructured LSC cathode showed the low resistance of 0.04 $\Omega \cdot cm^2$ at 700 °C in the air for 4000 h. However, the LSC perovskite-based cathode material cannot be widely used because it reacts rapidly with YSZ at 1000 °C, the required minimum sintering temperature to get ceramic bonding, to form insulating phases of lanthanum zirconia ($La_2Zr_2O_7$) and strontium zirconia ($SrZrO_3$) that in turn lower catalysis efficiency [57]. Therefore, infiltrating the LSC electrode can avoid this problem by decreasing the temperature of forming perovskite phase. The cell with a cathode composed of 30 vol. % LSC in a YSZ scaffold exhibited a peak power density of 2.1 $W \cdot cm^{-2}$ at 800 °C in hydrogen (H_2) [58].

Another promising material for high-performing cathode is rare earth element-based oxides such as barium strontium cobalt ferrite (BSCF) developed by Shao and Haile et al. Incorporated into a thin-film doped ceria single fuel cell, the electrode exhibited high power densities in the FC of 1010 $mW \cdot cm^{-2}$ at 600 °C and 402 $mW \cdot cm^{-2}$ at 500 °C when operated in humidified hydrogen and air [48]. The

area-specific resistance (ASR) was determined from the symmetric cell as remarkably as low between 0.055 and 0.071 $\Omega \cdot cm^2$ at 600 °C and between 0.51 and 0.6 $\Omega \cdot cm^2$ at 500 °C. The mechanism responsible for the increased performance was hypothesized from the oxygen permeation measurement. The high oxygen diffusivity through BSCF bulk yields its high rate of oxygen electrooxidation, while oxygen surface exchange process is the rate limiting step at low operating temperatures. Therefore, the superior high-performing SOFC at low temperatures can be possible after implementing the nanostructured BSCF cathode. There are two general strategies to achieve the nanostructured BSCF electrodes based upon pulse laser deposition (PLD) and wet chemistry ion infiltration method. Because of the low electrical conductivity of BSCF limiting the cathode catalysis activity, the thin catalyst layer is believed to enhance the ORR. Liu and Cheng et al. fabricated 800-nm-thick BSCF layer consisted of small nanoparticles with average particle size of about 40 nm onto YSZ/nickel oxide (NiO)-YSZ composite substrate with increased FC performance [59].

The nanoparticles grow to a dense layer on the YSZ electrolyte with agglomerated grains with characteristic diffraction peaks representing the {110}, {211}, {220}, and {310} crystal planes. The maximum power density with PLD-prepared BSCF cathode was 1.12 $W \cdot cm^{-2}$ in H_2 at 800 °C, compared with 0.45 $W \cdot cm^{-2}$ for conventional screen-printing BSCF cathode. With the infiltration of the stoichiometric metal salt solution, ~20 wt % BSCF nanoparticles with size about ~30 nm were formed on the surface of scaffold particles [60]. For the infiltrated composite cathode, the ORR occurred not only at the TPB but also at the prolonged cathode surface. It is found that electrode polarization resistance (R_p) reached the minimum value when the backbone is infiltrated with 16.2 wt % BSCF, e.g., 0.043 $\Omega \cdot cm^2$ at 700 °C.

The nanostructured BSCF electrode was also achieved by depositing other kinds of nanoparticles such as LSM or Ag onto the BSCF backbone [61, 62]. For example, the R_p of 1.8 $mg \cdot cm^{-2}$ BSCF-impregnated LSM cathode was 0.18 $\Omega \cdot cm^2$ at 800 °C, which its resistance was about 12 times lower than that of pure LSM, leading to increased FC performance. The YSZ electrolyte-based single cell with the nanostructured BSCF/LSM cathode exhibited maximum power densities of 1.21 and 0.32 $W \cdot cm^{-2}$ at 800 and 650 °C, respectively.

Strontium-doped samarium cobaltite (SSC) as a compositional cathode material has been extensively investigated by researchers for SOFC with different electrolytes [63–65]. Xia et al. found that the composite cathode of SSC and samarium-doped ceria (SDC, 10 wt %) significantly reduced the interfacial resistance from 2.0 $\Omega \cdot cm^2$ for pure SSC to less than 0.18 $\Omega \cdot cm^2$ at 600 °C under open circuit potential (OCP) condition. With combustion chemical vapor deposition (CVD) method, the composite cathode particles (70 wt % SSC and 30 wt % SDC) were about 50 nm in diameter. The electrode/electrolyte interfacial resistance is about 0.17 $\Omega \cdot cm^2$ at 600 °C. The maximum power densities were 60, 108, 159, 202, and 243 $mW \cdot cm^{-2}$ at 500, 550, 600, 650, and 700 °C, respectively [66]. Xia et al. also fabricated a nano-network of SSC by infiltration method for low-temperature SOFC. The nano-network consisted of well-connected SSC nanowires serving as conducting path for oxygen ion and

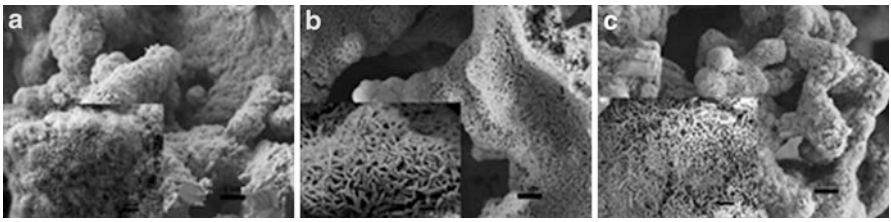

Fig. 8.3 Morphology of cathodes with impregnated SSC nanoparticles fired at different heating rates: (**a**) 5 °C min^{-1}; (**b**) 10 °C min^{-1}; (**c**) 30 °C min^{-1} [67]

electron conduction and catalysis sites, respectively [67]. The morphology was found to closely relate to a process of nucleation and growth affected by the heating rate (Fig. 8.3).

At a low heating rate, more time for solid nucleation and growth resulted in the formation of particles of large diameter that were distributed randomly on the outer surface of the SDC backbone frame, whereas with the higher heating rate, smaller diameter particles were generated due to the faster nucleation reaction, increased nucleation, and smaller nuclei nanoparticle clustering. The SSC nanoparticle formed a network as a cathode; the single cell with a nickel (Ni)-SDC anode and a 10-μm-thick SDC electrolyte showed peak power density of 0.44 W·cm^{-2} at 500 °C and 0.81 W·cm^{-2} at 600 °C.

8.3 Nanostructured Anode for Solid Oxide Fuel Cell (SOFC)

The SOFC anode is where the fuel (H_2, $C_xH_yO_z$, or NH_3) is oxidized by oxygen ions after electrons are released to pass the external circuit to form the electricity. In terms of fuel flexibility of SOFC, it is critical to developing a well-defined anode structure for high-performing SOFC. For over four decades, nickel-zirconia dual-phase cermet has been regarded as the dominant anode material. Nickel is an excellent metal catalyst for fuel oxidation, and Ni possesses a high degree of electronic conductance as an anode material. The reduction of NiO to Ni also produces a considerable amount of porosity for fuel gas diffusion. The use of zirconia is to provide ion conduction for extending sites of HOR and also to mechanically support the whole fuel cell. The importance of anode functioning as fuel oxidation chamber is mainly summarized in two aspects. Firstly, the anode performance using hydrogen fuel can be effectively improved by minimizing the polarization resistance when the microstructure of the anode is optimized because concentration polarization basically dominates the anode polarization. Meanwhile, as a place where the internal reforming takes place when the anode is fed with hydrocarbon fuels, the choice of anode material and decoration of microstructure with metals are critical to developing stable and high-performing anode in such fuels. Secondly, nickel-free ceramic oxides have also been studied as alternative anode materials. Due to low electrical conductivity and sluggish catalytic activity,

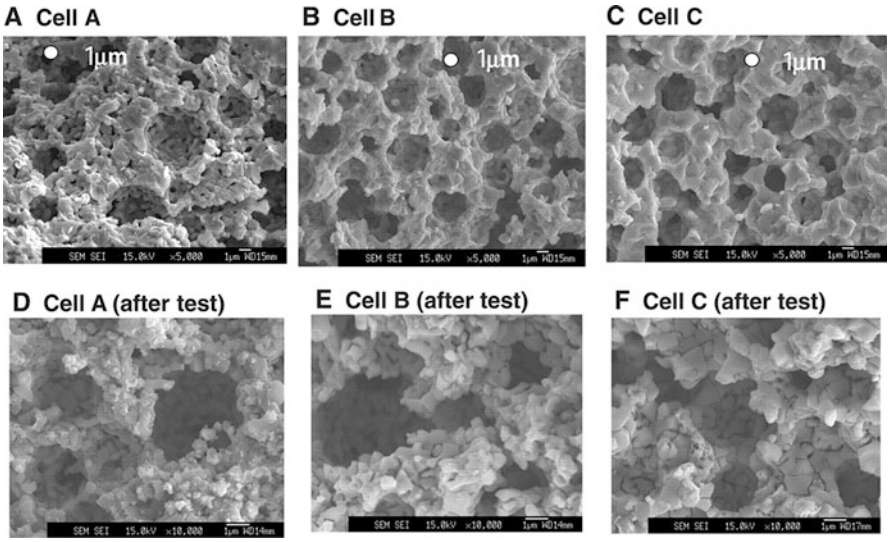

Fig. 8.4 Scanning electron microscopy images of Ni-YSZ anode microstructure before and after test [68]

the optimization of anode property and morphology is necessary to improve the anode performance. Therefore, the nanostructured anode for SOFC is discussed for nickel-based and nickel-free-based anode, respectively.

8.3.1 Nanostructured Nickel-Based Anode

Since nickel is the sole catalyst for fuel oxidation while the ceramic phase provides only mechanical support for the fuel cell, decreasing the anode particle size can significantly improve the electrochemical performance due to increased availability of reaction active sites. The effect of anode microstructure on SOFC performance has been studied by many researchers. Suzuki et al. correlated the microstructure of anode with electrochemical performance on a tubular SOFC design. With a conventional preparation method, the NiO-YSZ anode tube was prepared with high-porosity and nano-sized NiO particles (Fig. 8.4) [68]. Meanwhile, the YSZ electrolyte membrane was sintered on with a thickness only about 3 μm to minimize the ohmic resistance of the whole cell. The SOFC had a peak power density of more than 1 $W \cdot cm^{-2}$ at 600 °C.

The investigation of the hydrogen fuel flow rate affecting performance was performed to better understand the relationship between structure and SOFC power output. Zhan and Barnett et al. fabricated a thin LSGM electrolyte-based SOFC with nanostructured nickel oxide using a three-step procedure which employed (1) ion impregnation method to generate nano-catalyst [69], (2) depositing of a 30 μm LSGM layer onto LSGM dense pellet to form bilayer electrolyte/support

structure and sintering cathode and current collector layers, and (3) impregnation of the nickel nitrate solution into the porous LSGM structure and calcination at 700 °C in the air to generate a thin layer of NiO nanoparticles on the LSGM structure surface. The Ni loading was controlled by varying the impregnation cycles and solution concentration. The nanostructured SOFC showed high power densities of 1.20 $W \cdot cm^{-2}$ at 650 °C and 0.39 $W \cdot cm^{-2}$ at 550 °C when operated using humidified hydrogen as a fuel and air as an oxidant. The average diameters of synthesized Ni particles varied from ~30 nm when Ni volume loading is about 0.84% to ~90 nm at 2.51 vol. %. The increase in particle size was caused by repeated calcination cycles; therefore, it was a compromise between Ni loading and thermal cycle to yield the optimal performance. Some more dedicated studies further clarified the role of the nanostructured anode in the high-performance fuel cell by comparing the effect of anode functional layer located at TPB active area on decreasing cell polarization resistance. Park and Son et al. investigated the impact of a nanostructured Ni-YSZ anode on low-temperature SOFC performance by modifying the processing (ALD) technique to fabricate an anode-supported cells based on thin-film (~1 μm) electrolyte with and without the nanostructured Ni-YSZ anode. The Ni-YSZ anode functional layer with grain size about ~100 nm was fabricated [70]. It was determined that the anode with functional nano-sized particles increased FC significantly performance, particularly at a low temperature of 500 °C. The electrochemical analysis also revealed that the TPB density was increased near the electrolyte/anode interface because of increased number of active sites for charge transfer and fuel oxidation reaction. Their work also demonstrated that while cathode resistance was considered as the main factor in determining whole cell resistance, the anode structure could also affect the low-temperature performance. Yamaguchi and Barnett et al. also studied the nanostructured anode functional layer thickness playing a role in gaining better contact resistance [71]. With a thicker functional layer, the power density was gradually improved; and it was expected that the porosity of the catalytic layer started to be a negative effect on FC performance when the layer thickness was further increased to some threshold value, which has not been optimized.

8.3.2 Nanostructured Cu-Based Anode

As conventional nickel anode are vulnerable to hydrocarbon fuels when fuels are not reformed either internally or externally, alternative anode materials are proposed to replace potential problems such as coking and/or sulfur poisoning. One method proved to be an effective anode was anode containing copper due to the metals high electronic conductivity for fuel oxidation reaction and is inertness to coking. Therefore, a Cu anode can effectively inhibit carbon deposition and minimize degradation in catalysis. However, Cu anode is not active toward fuel catalysis; therefore, other forms of catalyst should be implemented into anode structure. Gorte et al. proposed a Cu-based anode with ceria nanoparticles for a direct-methane SOFC [72]. Because the melting temperature of CuO is as low as 1235 °C, the anode cermet co-sintering method cannot be used to prepare CuO-ceria composite anode at high sintering

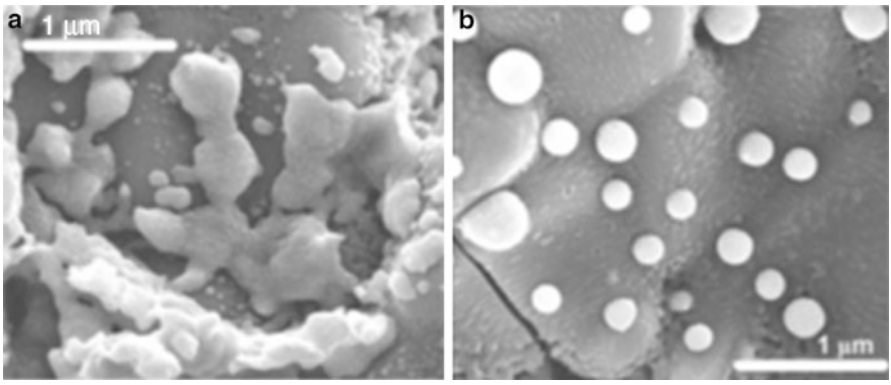

Fig. 8.5 SEM images of a Cu-CeO2-YSZ composite (18 vol% Cu, 9 vol% ceria) reduced in H_2 at (**a**) 700 °C and (**b**) 900 °C [73]

temperature for densifying the electrolyte membrane [73,74]. Therefore, the YSZ anode backbone was prepared by tape casting to form the porous structure after pre-sintering, and then Cu was added by aqueous impregnation with a concentrated solution of $Cu(NO_3)_2$, followed by firing in the air to form the nanoparticles (Fig. 8.5).

With a 60-μm-thick YSZ electrolyte and Cu-ceria anode, the cell was demonstrated to show direct oxidation of various hydrocarbons (methane, ethane, 1-butene, n-butane, and toluene) with products of carbon dioxide (CO_2) and water. The maximum power densities were 0.34 $W{\cdot}cm^{-2}$ for H_2 and 0.18 $W{\cdot}cm^{-2}$ for n-butane at 800 °C. Because Cu was used primarily as the current collector and ceria (CeO_2) for catalytic activity for fuel oxidation reaction, the infiltration of ceria was necessary to construct a catalytically active nanostructured Cu-ceria anode [75]. Some other metal-phase catalysts were also added into Cu-ceria anode by infiltration method to show more promise when the anode was operated using methane as a fuel feedstock [76].

8.3.3 Nanostructured Ceramic Oxide Anode

Several ceramic oxides with a perovskite structure have been extensively studied for alternative anode materials, which are mixed ionic-electronic conductors in the anodic conditions and catalytically even more active than ceria for oxidation of various fuels. Perovskites could readily accept oxygen vacancies and contain transition-metal cations in the octahedral sites due to their high tolerance against crystal distortion. Based on these several oxide-based perovskites, such as lanthanum strontium chromium manganite type (LSCM, $La_{0.75}Sr_{0.25}Cr_{0.5}Mn_{0.5}O_3$) [77] with other metals such as lanthanum strontium titanium oxide type (LSTO, $La_{0.33}Sr_{0.67}Ti_{1-x}M_xO_3$, where M was either titanium (Ti), iron (Fe^{n+}), manganese (Mn^{n+}), or scandium (Sc)) [78], nonstoichiometric ordered perovskite strontium

molybdate-type transition metal oxides Sr_2MMoO_6 (SMMO, where *M* is either magnesium (Mg), iron (Fe), or cobalt (Co)) [33, 79, 80] and praseodymium strontium niobium-type oxides (PSNO) with cobalt or iron ($Pr_{0.8}Sr_{1.2}(Co, Fe)_{0.8}Nb_{0.2}O_4$) [81] have been investigated as the potential anode materials. These conductive anode materials have high resistance against both coking and sulfur poisoning and limited stability under reducing condition. However, these anodes also showed other limitations, such as insufficient electrical conductivity and low catalytic activity when compared to those of the conventional Ni-YSZ anode. For instance, pure perovskite lanthanum strontium titanium-type oxide (LSTO) or lanthanum and strontium chromium-type manganite (LSCM) anode without a palladium (Pd) or nickel (Ni) catalyst provided lower catalytic performance using H_2 as a fuel source below 900 °C, and the anode catalytic activity toward CH_4 oxidation was also lower than with the anodes with the Ni catalyst [82,83]. It was further observed that the catalytic pathways for reforming methane during the cell operation could be blocked by the residual strontium carbonate ($SrCO_3$) and strontium molybdate ($SrMoO_4$) on the surface of the SMMO anode [84]. To enhance the performance of the FC using hydrogen and other fuels, it was hypothesized that nanostructuring of the ceramic oxide anode was able to significantly increase the number of active sites on functional nanoparticles catalyst that lead to increased performance.

8.3.3.1 Precious Metal

The impregnation of highly catalytic precious metals can enhance the performance of ceramic oxide anodes. The commonly used catalysts are a ruthenium (Ru), Pt, and Pd. The impregnated anodes demonstrate enhanced catalytic activity to fuel oxidation reaction. S. P. Jiang et al. [85] and Y. Ye et al. [86] both fabricated anodes with Pd nanoparticles by ion infiltration method, followed by determination of the electrocatalytic activity of composite LSCM/YSZ anode for the methane and ethanol oxidation reaction, which was significantly improved. At 800 °C, the electrode polarization resistance for methane oxidation was reduced by a factor of 3 with 0.1–0.66 mg·cm^2 loading of Pd. Kinetic analyses indicated that the oxygen transfer and methane decomposition processes were also promoted. It was determined that impregnation of Pd had a negligible effect on hydrogen oxidation using wet H_2. The study reported by R. J. Gorte et al. also investigated the improvement of catalysis by LSCM/YSZ anode by infiltrating different catalysts of Pt, Ni, Pd, and ceria [82]. For comparison, the electrode impedance (e.g., 1.5 Ω·cm^2) was measured for a variety of anode materials without and with a metal catalyst. The resistance decreased to 0.36 Ω·cm^2 with the addition of 5 wt % ceria and to 0.08 Ω·cm^2 with 0.5 wt % Pd and 5 wt % ceria. It is hypothesized that the metals Pd or Pt primarily enhance the diffusion and dissociation related with electrode processes at low frequencies in impedance spectra, which facilitates the mass transfer of reaction species. The combination of ceria and Pd or Pt nanoparticles can further enhance the performance of the anode. For example, Ru-CeO_2 (50%) and YST ($Sr_{0.88}Y_{0.08}TiO_3$) (50%) anode YSZ ($Y_{0.08}Zr_{0.92}O_2$) electrolyte exhibited peak power densities of 510 mW·cm^{-2} in H_2 and 470 mW·cm^{-2} in H_2 with 10 ppm H_2S at 800 °C [87].

8.3.3.2 Non-precious Metal

One major drawback of fuel cell-related manufacturing costs is related to the cost of utilization of precious metal catalysts. The cost could be lowered by substitution of the precious metals by catalytically active non-precious metal in the electrode as demonstrated by Liu [88]. Uchida et al. [89] introduced a small amount of Ni catalyst (6–8 vol. %) into the ceramic frame for increasing the active area for reaction significantly. Fu and Irvine found that yttrium-substituted $SrTiO_3$ (YST) was a very good electronic conductor with conductivity about 20–100 $S{\cdot}cm^{-2}$ at 800 °C but showed limited catalytic activity [90]. By implementing the required ionic conductivity and catalytic activity, YSZ was combined with YST to supply the ionic conduction path, and the composite material was fabricated as the ceramic frame. A small amount of Ni catalyst was incorporated into the two-phase ceramic network to enhance the reaction activity. The R_p with 0%, 5%, and 10% Ni loaded into YST/YSZ anodes in wet 5% hydrogen (H_2)/balanced by argon (Ar) at 850 °C was determined, and the anode showed a decreasing trend in ohmic resistance from 0.49 to 0.17 and then 0.13 $\Omega{\cdot}cm^2$, respectively [90]. The Ni nanoparticles with a size of 50–100 nm were fabricated to potentially offer a large number of active sites for the HOR, and it was determined that the nanoparticles were effectively separated by strontium yttria titania (SYT)/yttria-stabilized zirconia (YSZ) particles with a minor degree of grain coarsening. The Ni nanoparticles were also employed into different ceramic anodes. Boulfrad and Irvine et al. coated 5 wt % nickel onto lanthanum strontium chromium manganese oxide-type (LSCM, $La_{0.75}Sr_{0.25}Cr_{0.5}Mn_{0.5}O_{3-\delta}$) perovskite particles to form the nanostructured ceramic oxide particles which are then mixed with different amounts of gadolinium-doped ceria (CGO, $Ce_{0.9}Gd_{0.1}O_{1.95-\delta}$) material as the anode [91]. Under examinations of scanning transmission electron microscopy (STEM) and X-ray energy dispersive spectroscopy (EDS), nickel was observed to be precipitated in the form of nanoparticles under reducing condition. The Ni nanoparticles led to a decrease in anodic activation energy by half, and the electrode polarization resistance also dropped by 60% at 800 °C. Yoo et al. reported a maximum power density of ~0.63 $W{\cdot}cm^{-2}$ in H_2 at 800 °C for a lanthanum strontium gallium magnesium oxide (LSGM)-type (~250 μm) electrolyte-supported SOFC with Ni-impregnated lanthanum gallate, strontium, and titanium cobaltite-gadolinium-doped ceria-type ($(La_{0.2}Sr_{0.8}Ti_{0.98}Co_{0.02}O_3)$-Ni-GDC) composite anode [92].

Xiao and Chen et al. used temperature-programed reduction (TPR) technique to study the promotion effect of Ni (~2 wt %) on hydrogen oxidation when it is infiltrated onto a double perovskite strontium ferrite molybdate (SFM, $Sr_2Fe_{1.5}Mo_{0.5}O_6$) ceramic anode [93]. With the Ni-modified SFM anode, the metal reduction signal starts to shift toward lower temperature, indicating the interaction between Ni hydrogen increased. The scanning electron microscopy (SEM) analyses during the reduction process indicated that the oxidation of hydrogen was more facile. A cell with nickel-strontium ferrite molybdate (Ni-SFM) as the anode, lanthanum strontium gallium magnesium oxide type (LSGM, $La_{0.8}Sr_{0.2}Ga_{0.83}Mg_{0.17}O_3$) as the electrolyte, and lanthanum strontium

cobalt ferrite type (LSCF, $La_{0.6}Sr_{0.4}Co_{0.2}Fe_{0.8}O_3$) as the cathode showed a high peak power density of 1166 $mW{\cdot}cm^{-2}$ at 800 °C using H_2 as the fuel and ambient air as the oxidant. The cell polarization resistance is only about 0.145 $\Omega{\cdot}cm^2$ at 800 °C which was much lower than that of the cell with pure SFM anode (0.243 $\Omega{\cdot}cm^2$) under the same testing conditions. However, it was also found that SFM anode with dispersive Ni on the surface could be poisoned by trace levels of hydrogen sulfide (H_2S) in the fuel. The current density of the cell operated at a constant voltage of 0.7 V at 800 °C in H_2 with 100 parts-per-million (ppm) H_2S dropped from 1.34 to 1.1 $A{\cdot}cm^{-2}$ after 20 h continuous operation. Such as fast degradation rate was much higher than that observed in SFM without Ni coating. Therefore, there modified Ni-modified SFM anode demonstrated limitations on the Ni before the H_2S-poisoning problem was solved.

Some other transition metals such as Co, Fe, or Co-Fe were also reported to be used in enhancing the SOFC anode performance by infiltration and in situ precipitation from the surface. For example, Yang and Chen et al. reported a composite anode consisting of potassium tetrafluoride nickelate (II) (K_2NiF_4)-type-structured praseodymium strontium cobalt iron-doped niobium oxide-type (K-PSCFN, $Pr_{0.8}Sr_{1.2}(Co, Fe)_{0.8}Nb_{0.2}O_{4+\delta}$) matrix with homogeneously dispersed nano-sized Co-Fe alloy by annealing the perovskite praseodymium strontium cobalt iron-doped niobium oxide-type (P-PSCFN, $Pr_{0.4}Sr_{0.6}Co_{0.2}Fe_{0.7}Nb_{0.1}O_{3-\delta}$) using H_2 at 900 °C [81]. The fabricated Co-Fe nanostructured ceramic anode was demonstrated to yield comparable performance to the Ni-based cermet anode with enhanced sulfur tolerance and coking resistance. In pure H_2, the electrolyte-supported cell with a structure of K-PSCFN-cobalt iron alloy (CFA)|LSGM|P-PSCFN electrolyte showed a maximum power density of 0.96 $W{\cdot}cm^{-2}$ at 850 °C, compared with 0.21 $W{\cdot}cm^{-2}$ without the Co-Fe catalyst. The cell also exhibited high power density using H_2 fuel containing H_2S of 0.92 $W{\cdot}cm^{-2}$ at 50 ppm H_2S and of 0.89 $W{\cdot}cm^{-2}$ at 100 ppm H_2S operated at 850 °C. The results demonstrate the impact of Co-Fe alloying on the catalytic activity of ceramic anode. The Co-Fe nanostructured anode also showed long-term stability in H_2S-containing fuel and hydrocarbon fuels (CH_4 and C_3H_8) when the cell was discharged at different constant voltages. The redox cyclic stability of the anode was examined by switching the gas at anode side from H_2 to air repeatedly to show the reversibility of the Co-Fe alloy. A study by G. Kim et al. recently developed a double perovskite material containing praseodymium barium magnesium oxide type (PBMO, $PrBaMn_2O_{5+\delta}$) as a ceramic anode for high-performing direct hydrocarbon SOFC [94]. The PBMO anode was prepared by in situ annealing PBMO perovskite under reducing condition. With a 15 wt % Co-Fe catalyst under humidified H_2, C_3H_8, and CH_4 fuels (3% H_2O), the single cell exhibited peak power densities of 1.77, 1.32, and 0.57 $W{\cdot}cm^{-2}$ at 850 °C using humidified hydrogen and propane fuels, respectively.

8.3.3.3 Ceramic Oxides

The incorporation of ceramic anode nanoparticles into the anode is complicated due to the difficulty of infiltrating multiple metal ions into the ceramic structure and

forming the correct phase structure after treatment. The fabricated nanostructured ceramic anodes exhibit a longer TPB length by extending the oxide catalyst throughout the electrode. Lee and Gorte et al. infiltrated 45 wt % lanthanum strontium gallium titanium oxide type (LST, $La_{0.3}Sr_{0.7}TiO_3$) into 65% porous YSZ electrode scaffold to form the composite anode. The microstructure of infiltrated anode was greatly affected by the calcination temperature [95]. With conductivity of 0.4 S/cm at 900 °C in H_2 comparable to traditional anodes, however, the cell (LST-YSZ anode | YSZ electrolyte ~60 μm | LSF-YSZ cathode) operated in humidified H_2 at 800 °C showed only a peak power density of 20 $mW{\cdot}cm^{-2}$. With the addition of 5% ceria and 0.5 wt % Pd, the power density was dramatically increased to 780 $mW{\cdot}cm^{-2}$, indicating the low electrochemical activity for hydrogen oxidation by LST itself. Lack of catalytic activity after infiltrating the ceramic catalyst nanoparticles also occurred on the LSCM anode, owing to its low electrical conductivity [96–99]. By infiltrating 45 wt % LSCM into a porous YSZ layer, the power density of the SOFC with 60-μm-thick YSZ electrolyte reached 500 $mW{\cdot}cm^{-2}$ in H_2 at 700 °C with the addition of 0.5–1% Pd, rhodium (Rh), or Ni metals as catalysts. Therefore, the catalytic activity of the ceramic oxide itself was critical in obtaining comparable performance with Ni-based cermet anode. Recently, Ding and Zhang et al. reported a highly redox-stable ceramic oxide with an *A*-site-deficient layered perovskite structure, praseodymium barium ferrite magnesium oxide type $(PrBa)_{0.95}(Fe_{0.9}Mo_{0.1})O_{5+\delta}$ (PBFM), as the anode material in a direct methane-fueled SOFC [100]. Firstly, the selection of this material was based on four general considerations. (1) Perovskites with high tolerance against crystal structure distortion could fine-tune the material's chemical stability and also the electrical/catalytic/mechanical properties through doping strategy; (2) iron-rich perovskite containing mixed-valence Fe^{2+}/Fe^{3+} redox couple could provide high electronic conductivity even though these redox ions only partially occupy the sub-lattice; (3) layered perovskite structure could be fabricated to yield high electrical conductivity and the ordered *A*-cations localizing oxygen vacancies within the rare earth layers, which could make a contribution to fast oxygen surface exchange/bulk diffusion and catalytic activity toward both hydrogen and hydrocarbon oxidation processes; and (4) our experiments lead us to hypothesize that the PBFM perovskites are stable upon partial removal of lattice oxygen and that the use of sixfold-coordinated Mo (VI)/Mo(V) couple at the *B* site could stabilize the material with stronger chemical bond under crude anodic conditions. The single cell of a lanthanum strontium gallium magnesium oxide-type (LSGM, $La_{0.8}Sr_{0.2}Ga_{0.8}Mg_{0.2}O_{2.8}$) electrolyte-supported SOFC with the configuration of praseodymium barium ferrite magnesium oxide type (PBFM), LSGM, and praseodymium barium cobaltite type (PBCO, $PrBaCo_2O_{5+\delta}$) [PBFM|LSGM|PBCO] showed maximum power densities of 1.72, 1.05, and 0.56 $W{\cdot}cm^{-2}$ at 800, 700, and 600 °C, respectively. The PBFM anode was nanostructured by infiltrating the nitrates solution with the same stoichiometry as the prime backbone material. The as-prepared cell showed an enhanced performance, for example, the power densities of 2.3, 1.5, and 0.8 $W{\cdot}cm^{-2}$ at 800, 700, and 600 °C in H_2 were achieved, respectively.

8.4 Conclusion

Nano-engineering electrodes for SOFC operating in various fuels at intermediate temperatures through ion impregnation method to increase the catalysis active sites for ORR or fuel oxidation reaction have become a crucial strategy in enhancing FC performance. The optimization of the electrode microstructure can effectively minimize the activation polarization resistance when the nano-sized particles were incorporated into the electrode scaffold. There have been extensive studies focusing on the addition of different types of functional catalyst into electrodes. The research findings indicate that the nano-engineering electrode was a very promising route to facilitate the intermediate temperature operation of SOFC, while new material development was also under way.

References

1. N.Q. Minh, Ceramic fuel cells. J. Am. Ceram. Soc. **76**, 563–588 (1993)
2. A.J. Jacobson, Materials for solid oxide fuel cells. Chem. Mater. **22**, 660–674 (2010)
3. D.J.L. Brett, A. Atkinson, N.P. Brandon, S.J. Skinner, Intermediate temperature solid oxide fuel cells. Chem. Soc. Rev. **37**, 1568–1578 (2008)
4. R.M. Ormerod, Solid oxide fuel cells. Chem. Soc. Rev. **32**, 17–28 (2003)
5. Y. Yi, A.D. Rao, J. Brouwer, G.S. Samuelsen, J. Power Sources **144**, 67–76 (2005)
6. S.C. Singhal, Solid oxide fuel cells for stationary, mobile, and military applications. Solid State Ionics **152-153**, 405–410 (2002)
7. W.G. Coors, Protonic ceramic fuel cells for high-efficiency operation with methane. J. Power Sources **118**, 150–156 (2003)
8. L. Yang, C.D. Zuo, S.Z. Wang, Z. Cheng, M. Liu, A novel composite cathode for low-temperature SOFCs based on oxide proton conductors. Adv. Mater. **20**, 3280–3283 (2008)
9. N.M. Sammes, Y. Du, R. Bove, Design and fabrication of a 100 W anode-supported tubular SOFC stack. J. Power Sources **145**, 428–434 (2005)
10. T. Fukui, S. Ohara, K. Mukai, Long-term stability of Ni-YSZ anode with a new microstructure prepared from composite powder. Electrochem. Solid-State Lett. **29**(1), 120–122 (1998)
11. A. Atkinson, S. Barnett, R.J. Gorte, J.T.S. Irvine, A.J. McEvoy, M. Mogensen, S.C. Singhal, J. Vohs, Advanced anodes for high-temperature fuel cells. Nat. Mater. **3**, 17–27 (2004)
12. T. Zhang, W.G. Fahrenholtz, S.T. Reis, R.K. Brow, Borate volatility from SOFC sealing glasses. J. Am. Ceram. Soc. **91**, 2564–2569 (2008)
13. E.P. Murray, T. Tsai, S.A. Barnett, A direct-methane fuel cell with a ceria-based anode. Nature **400**, 649–651 (1999)
14. S. McIntosh, R.J. Gorte, Direct hydrocarbon solid oxide fuel cells. Chem. Rev. **104**, 4845–4865 (2004)
15. Y.H. Huang, R.I. Dass, Z.L. Xing, J.B. Goodenough, Double perovskites as anode materials for solid oxide fuel cells. Science **312**, 254–257 (2006)
16. R. Steinberger-Wilckens, F. Tietz, M.J. Smith, J. Mougin, B. Rietveld, O. Bucheli, J.V. Herle, R. Rosenberg, M. Zahid, P. Holtappels, Real-SOFC–a joint European effort in understanding SOFC degradation. ECS Trans. **7**, 67–76 (2007)
17. A. Hagen, R. Barfod, P.V. Hendriksen, Y.-L. Liu, S. Ramousse, Degradation of anode-supported SOFCs as a function of temperature and current load. J. Electrochem. Soc. **153**, A1165–A1171 (2006)

18. M.L. Liu, M.E. Lynch, K. Blinn, F.M. Alamgir, Y.M. Choi, Rational SOFC material design: new advances and tools. Mater. Today **14**, 534–546 (2011)
19. J.-H. Lee, J.-W. Heo, D.-S. Lee, J. Kim, G.-H. Kim, H.-W. Lee, H.S. Song, J.-H. Moon, The impact of anode microstructure on the power generating characteristics of SOFC. Solid State Ionics **158**, 225–232 (2003)
20. K.J. Yoon, P. Zink, S. Gopalan, U.B. Pal, Polarization measurements on single-step co-fired solid oxide fuel cells (SOFCs). J. Power Sources **172**, 39–49 (2007)
21. A.V. Virkar, J. Chen, C.W. Tanner, J.-W. Kim, The role of electrode microstructure on activation and concentration polarizations in solid oxide fuel cells. Solid State Ionics **131**, 189–198 (2000)
22. S.H. Chan, K.A. Khor, Z.T. Xia, A complete polarization model of a solid oxide fuel cell and its sensitivity to the change of cell component thickness. J. Power Sources **93**, 130–140 (2001)
23. D.A. Noren, M.A. Hoffman, Clarifying the Butler-Volmer equation and related approximations for calculating activation losses in solid oxide fuel cell models. J. Power Sources **152**, 175–181 (2005)
24. Z.P. Shao, S.M. Haile, A high-performance cathode for the next generation of solid-oxide fuel cells. Nature **431**, 170–173 (2004)
25. S.B. Adler, Factors governing oxygen reduction in solid oxide fuel cell cathodes. Chem. Rev. **104**, 4791–4843 (2004)
26. C.W. Sun, R. Hui, J. Roller, Cathode materials for solid oxide fuel cells: a review. J. Solid State Electrochem. **14**, 1125–1144 (2010)
27. S.J. Skinner, Recent advances in perovskite-type materials for solid oxide fuel cell cathodes. Int. J. Inorg. Mater. **3**, 113–121 (2001)
28. A. Tarancón, S.J. Skinner, R.J. Chater, F. Hernández-Ramírez, J.A. Kilner, Layered perovskites as promising cathodes for intermediate temperature solid oxide fuel cells. J. Mater. Chem. **17**, 3175–3181 (2007)
29. L. Shao, Q. Wang, L. Fan, P. Wang, N. Zhang, K. Sun, Copper-cobalt spinel as a high-performance cathode for intermediate temperature solid oxide fuel cells. Chem. Commun. **52**, 8615–8618 (2016)
30. Q. Fu, F. Tietz, D. Sebold, S. Tao, J.T.S. Irvine, An efficient ceramic-based anode for solid oxide fuel cells. J. Power Sources **171**, 663–669 (2007)
31. G. Xiao, F. Chen, Redox stable anodes for solid oxide fuel cells. Front. Energy Res. **2**, 1–13 (2014)
32. K. Huang, J. Wan, J.B. Goodenough, Oxide-ion conducting ceramics for solid oxide fuel. Cell **36**, 1093–1098 (2001)
33. J.B. Goodenough, Y.-H. Huang, Alternative anode materials for solid oxide fuel cells. J. Power Sources **173**, 1–10 (2007)
34. P.G. Bruce, B. Scrosati, J.-M. Tarascon, Nanomaterials for rechargeable lithium batteries. Angew. Chem. **47**, 2930–2946 (2008)
35. L. Zhang, T.J. Webster, Nanotechnology and nanomaterials: promises for improved tissue regeneration. Nano Today **4**, 66–80 (2009)
36. Q. Peng, Y.-C. Tseng, S.B. Darling, J.W. Elam, A route to nanoscopic materials via sequential infiltration synthesis on block copolymer templates. ACS Nano **5**, 4600–4606 (2011)
37. J. Martin, C. Mijangos, Tailored polymer-based nanofibers and nanotubes by means of different infiltration methods into alumina nanopores. Langmuir **25**, 1181–1187 (2009)
38. T.Z. Sholklapper, H. Kurokawa, C.P. Jacobson, S.J. Visco, L.C. De Jonghe, Nanostructured solid oxide fuel cell electrodes. Nano Lett. **7**, 2136–2141 (2007)
39. C.C. Chao, C.M. Hsu, Y. Cui, F.B. Prinz, Improved solid oxide fuel cell performance with nanostructured electrolytes. ACS Nano **5**, 5692–5696 (2011)
40. L. Baque, A. Caneiro, M.S. Moreno, A. Serquis, High-performance nanostructured IT-SOFC cathodes prepared by the novel chemical method. Electrochem. Commun. **10**, 1905–1908 (2008)

41. D. Ding, X. Li, S.Y. Lai, K. Gerdes, M. Liu, Enhancing SOFC cathode performance by surface modification through infiltration. Energy Environ. Sci. **7**, 552–575 (2014)
42. J.M. Vohs, R.J. Gorte, High-performance SOFC cathodes prepared by infiltration. Adv. Mater. **21**, 943–956 (2009)
43. S.P. Jiang, A review of wet impregnation – an alternative method for the fabrication of high performance and nanostructured electrodes of solid oxide fuel cells. Mater. Sci. Eng. **418**, 199–210 (2006)
44. S.P. Jiang, Nanoscale and nanostructured electrodes of solid oxide fuel cells by infiltration: advances and challenges. Int. J. Hydro. Energy **37**, 449–470 (2012)
45. M.J. Jorgensen, M. Mogensen, Impedance of solid oxide fuel cell LSM/YSZ composite cathodes. J. Electrochem. Soc. **148**, A433–A442 (2001)
46. M. Shiono, K. Kobayashi, T.L. Nguyen, K. Hosoda, T. Kato, K. Ota, M. Dokiya, Effect of the CeO_2 interlayer on ZrO_2 electrolyte/la(Sr)CoO_3 cathode for low-temperature SOFCs. Solid State Ionics **170**, 1–7 (2004)
47. L. Yang, C.D. Zuo, S.Z. Wang, Z. Cheng, M.L. Liu, A novel composite cathode for low-temperature SOFCs based on oxide proton conductors. Adv. Mater. **20**, 3280–3283 (2008)
48. Z.P. Shao, S.M. Haile, A high-performance cathode for the next generation of solid-oxide fuel cells. Nature **431**, 170–173 (2004)
49. H. He, Y. Huang, J. Regal, M. Boaro, J.M. Vohs, R.J. Gorte, Low-temperature fabrication of oxide composites for solid-oxides fuel cells. J. Am. Ceram. Soc. **87**, 331–336 (2004)
50. Y. Huang, J.M. Vohs, R.J. Gorte, Characterization of LSM-YSZ composites prepared by impregnation methods. J. Electrochem. Soc. **152**, A1347–A1353 (2005)
51. T.J. Armstrong, A.V. Virkar, *204th Meeting of the Electrochemical Society* (Electrochemical Society, Pennington, 2003). Abstract 1113
52. Z. Jiang, Z. Lei, B. Ding, C. Xia, F. Zhao, F. Chen, Electrochemical characteristics of solid oxide fuel cell cathodes prepared by infiltrating (la,Sr)MnO3 nanoparticles into yttria-stabilized bismuth oxide backbones. Int. J. Hydrog. Energy **35**, 8322–8330 (2010)
53. T.Z. Sholklapper, C. Lu, C.P. Jacobson, S.J. Visco, L.C. De Jonghe, LSM-infiltrated solid oxide fuel cell cathodes. Electrochem. Solid-State Lett. **9**, A376–A378 (2006)
54. T.Z. Sholklapper, V. Radmilovic, C.P. Jacobson, S.J. Visco, L.C.D. Jonghe, Electrochem. Solid-State Lett. **10**, B74–B76 (2007)
55. M.G. Bellino, J.G. Scannell, D.G. Lamas, A.G. Leyva, N.E. Walsöe de Reca, High-performance solid-oxide fuel cell cathodes based on cobaltite nanotubes. J. Am. Chem. Soc. **129**, 3066–3067 (2007)
56. Y. Gong, D. Palacio, X. Song, R.L. Patel, X. Liang, X. Zhao, J.B. Goodenough, K. Huang, Stabilizing nanostructured solid oxide fuel cell cathode with atomic layer deposition. Nano Lett. **13**, 4340–4345 (2013)
57. Y.L. Liu, A. Hagen, R. Barfod, M. Chen, H.J. Wang, F.W. Poulsen, P.V. Hendriksen, Microstructural studies on the degradation of the interface between LM-YSZ cathode and YSZ electrolyte in SOFCs. Solid State Ionics **180**, 1298–1304 (2009)
58. T.J. Armstrong, J.G. Rich, Anode-supported solid oxide fuel cells with $La_{0.6}Sr_{0.4}CoO_{3-\delta}$-$Zr_{0.84}Y_{0.16}O_{2-\delta}$ composite cathodes fabricated by an infiltration method. J. Electrochem. Soc. **153**, A515–A520 (2006)
59. B. Liu, X. Chen, Y. Dong, S.S. Mao, M. Cheng, A high-performance, a nanostructured $Ba_{0.5}Sr_{0.5}Co_{0.8}Fe_{0.2}O_{3-\delta}$ cathode for solid oxide fuel cells. Adv. Energy Mater. **1**, 343–346 (2011)
60. D. Han, X. Liu, F. Zeng, J. Qian, T. Wu, Z. Zhan, A micro-nano porous oxide hybrid for efficient oxygen reduction in reduced-temperature solid oxide fuel cells. Sci. Rep. **2**, 462 (2012)
61. N. Ai, S.P. Jiang, Z. Lü, K. Chen, W. Su, Nanostructured (Ba,Sr)(Co,Fe) $O_{3-\delta}$ impregnated (La,Sr) MnO_3 cathode for intermediate-temperature solid oxide fuel cells. J. Electrochem. Soc. **157**, B1033–B1039 (2010)

62. R. Su, Z. Lü, S.P. Jiang, Y.B. Shen, W.H. Su, K.F. Chen, Ag decorated (Ba,Sr)(Co,Fe)O_3 cathodes for solid oxide fuel cells prepared by electroless silver deposition. Int. J. Hydrog. Energy **38**, 2413–2420 (2013)
63. C. Xia, M. Liu, A simple and cost-effective approach to fabrication of dense ceramic membranes on porous substrates. J. Am. Ceram. Soc. **84**, 1903–1905 (2001)
64. C. Xia, F. Chen, M. Liu, Reduced-temperature solid oxide fuel cells fabricated by screen printing. Electrochem. Solid-State Lett. **4**, A52–A54 (2001)
65. H.Y. Tu, Y. Takeda, N. Imanishi, O. Yamamoto, $Ln_{1-x}Sr_xCoO_3$ (Ln=Sm, Dy) for the electrode of solid oxide fuel cells. Solid State Ionics **100**, 283–288 (1997)
66. Y. Liu, S. Zha, M. Liu, Novel nanostructured electrodes for solid oxide fuel cells fabricated by combustion chemical vapor deposition (CVD). Adv. Mater. **16**, 256–260 (2004)
67. F. Zhao, Z. Wang, M. Liu, L. Zhang, C. Xia, F. Chen, Novel nano-network cathodes for solid oxide fuel cells. J. Power Sources **185**, 13–18 (2008)
68. T. Suzuki, Z. Hasan, Y. Funahashi, T. Yamaguchi, Y. Fujishiro, M. Awano, Impact of anode microstructure on solid oxide fuel cells. Science **325**, 852–855 (2009)
69. Z. Zhan, S.A. Barnett, A reduced temperature solid oxide fuel cell with nanostructured anodes. Energy Environ. Sic. **4**, 3951–3954 (2011)
70. J.H. Park, S.M. Han, K.J. Yoon, H. Kim, J. Hong, B.-K. Kim, J.-H. Lee, J.-W. Son, Impact of nanostructured anode on low-temperature performance of thin-film-based anode-supported solid oxide fuel cells. J. Power Sources **315**, 324–330 (2016)
71. T. Yamaguchi, H. Sumi, K. Hamamoto, T. Suzuki, Y. Fujishiro, J.D. Carter, S.A. Barnett, Effect of nanostructured anode functional layer thickness on the solid-oxide fuel cell performance in the intermediate temperature. Int. J. Hydrog. Energy **39**, 19731–19736 (2014)
72. S. Park, J.M. Vohs, R.J. Gorte, Direct oxidation of hydrocarbons in a solid-oxide fuel cell. Nature **404**, 265–267 (2000)
73. R.J. Gorte, S. Park, J.M. Vohs, C. Wang, Anodes for direct oxidation of dry hydrocarbons in a solid-oxide fuel cell. Adv. Mater. **12**, 1465–1469 (2000)
74. M.D. Gross, J.M. Vohs, R.J. Gorte, Recent progress in SOFC anodes for direct utilization of hydrocarbons. J. Mater. Chem. **17**, 3071–3077 (2007)
75. X.-F. Ye, B. Huang, S.R. Wang, Z.R. Wang, L. Xiong, T.L. Wen, Preparation and performance of a Cu–CeO_2–ScSZ composite anode for SOFCs running on ethanol fuel. J. Power Sources **164**, 203–209 (2007)
76. R.J. Gorte, J.M. Vohs, Nanostructured anodes for solid oxide fuel cells. Curr. Opin. Colloid Interface Sci. **14**, 236–244 (2009)
77. S.W. Tao, J.T.S. Irvine, A redox-stable efficient anode for solid oxide fuel cells. Nat. Mater. **2**, 320–323 (2003)
78. X.W. Zhou, N. Yan, K.T. Chuang, J.L. Luo, Progress in La-doped SrTiO3 (LST)-based anode materials for solid oxide fuel cells. RSC Adv. **4**, 118–131 (2014)
79. Y.H. Huang, R.I. Dass, Z.L. Xing, J. Goodenough, Double perovskites as anode materials for solid oxide fuel cells. Science **312**, 254–257 (2006)
80. Q. Liu, X.H. Dong, G.L. Xiao, F. Zhao, F.L. Chen, A novel electrode material for symmetric SOFCs. Adv. Mater. **22**, 5478–5482 (2010)
81. C.H. Yang, Sulfur-tolerant redox-reversible anode material for direct hydrocarbon solid oxide fuel cells. Adv. Mater. **24**, 1439–1443 (2012)
82. J.S. Kim, V.V. Nair, J.M. Vohs, R.J. Gorte, A study of the methane tolerance of LSCM-YSZ composite anodes with Pt, Ni, Pd and ceria catalysts. Scr. Mater. **65**, 90–95 (2011)
83. K.B. Yoo, G.M. Choi, LST-GDC composite anode on $LaGaO_3$-based solid oxide fuel cell. Solid State Ionics **192**, 515–518 (2011)
84. Y.H. Huang, Double-perovskite anode materials Sr_2MMoO_6 (M = Co, Ni) for solid oxide fuel cells. Chem. Mater. **21**, 2319–2326 (2009)
85. S.P. Jiang, Y. Ye, T. He, S.B. Ho, Nanostructured palladium–$La_{0.75}Sr_{0.25}Cr_{0.5}Mn_{0.5}O_3$/$Y_2O_3$–$ZrO_2$ composite anodes for direct methane and ethanol solid oxide fuel cells. J. Power Sources **185**, 179–182 (2008)

86. Y. Ye, T. He, Y. Li, E.H. Tang, T.L. Reitz, S.P. Jiang, Pd-promoted $La_{0.75}Sr_{0.25}Cr_{0.5}Mn_{0.5}O_3$/YSZ composite anodes for direct utilization of methane in SOFCs. J. Electrochem. Soc. **155**, B811–B818 (2008)
87. H. Kurokawa, J. Yang, C. Jacobson, L. DE Jongle, S. Visco, Y-doped $SrTiO_3$ based sulfur tolerant anode for solid oxide fuel cells. J. Power Sources **164**, 510–518 (2007)
88. S. Primdahl, Y.L. Liu, Ni catalyst for hydrogen conversion in Gadolinia-doped ceria anodes for solid oxide fuel cells. J. Electrochem. Soc. **149**, A1466–A1472 (2002)
89. H. Uchida, S. Suzuki, M. Watanabe, High performance electrode for medium-temperature solid oxide fuel cells. Electrochem. Solid-State Lett. **6**, A174–A177 (2003)
90. Q. Fu, F. Tietz, D. Sebold, S. Tao, J. Irvine, An efficient ceramic-based anode for solid oxide fuel cells. J. Power Sources **171**, 663–669 (2007)
91. S. Boulfrad, M. Cassidy, E. Traversa, J.T.S. Irvine, Improving the performance of SOFC anodes by decorating perovskite with Ni nanoparticles. ECS Trans. **57**, 1211–1216 (2013)
92. K.B. Yoo, B.H. Park, G.M. Choi, Stability and performance of SOFC with $SrTiO_3$-based anode in CH_4 fuel. Solid State Ionics **225**, 104–107 (2012)
93. G. Xiao, C. Jin, Q. Liu, A. Heyden, F. Chen, Ni modified ceramic anodes for solid oxide fuel cells. J. Power Sources **201**, 43–48 (2012)
94. S. Sengodan, S. Choi, A. Jun, T.H. Shin, Y.-W. Ju, H.Y. Jeong, J. Shin, J.T.S. Irvine, G. Kim, Layered oxygen-deficient double perovskite as an efficient and stable anode for direct hydrocarbon solid oxide fuel cells. Nat. Mater. **14**, 205–209 (2015)
95. S. Lee, G. Kim, J.M. Vohs, R.J. Gorte, SOFC anodes based on infiltration of La0.3Sr0.7TiO3. J. Electrochem. Soc. **155**, B1179–B1183 (2008)
96. G. Kim, S. Lee, J.Y. Shin, G. Corre, J.T.S. Irvine, J.M. Vohs, R.J. Gorte, Investigation of the structural and catalytic requirements for high-performance SOFC anodes formed by infiltration of LSCM. Electrochem. Solid-State Lett. **12**, B48–B52 (2009)
97. G. Corre, G. Kim, M. Cassidy, J.M. Vohs, R.J. Gorte, J.T.S. Irvine, Activation and ripening of impregnated manganese containing perovskite SOFC electrodes under redox cycling. Chem. Mater. **21**, 1077–1084 (2009)
98. G. Kim, G. Corre, J.T.S. Irvine, J.M. Vohs, R.J. Gorte, Engineering composite oxide SOFC anodes for efficient oxidation of methane. Electrochem. Solid-State Lett. **11**, B16–B19 (2008)
99. J.-S. Kim, N.L. Wieder, A.J. Abraham, M. Cargnello, P. Fornasiero, R.J. Gorte, J.M. Vohs, Highly active and thermally stable core-shell catalysts for solid oxide fuel cells. J. Electrochem. Soc. **158**, B596–B600 (2011)
100. H. Ding, Z. Tao, S. Liu, J. Zhang, A high-performing sulfur-tolerant and redox-stable layered perovskite anode for direct hydrocarbon solid oxide fuel cells. Sci. Rep. **5**, 18129 (2015)